Article:

Groom, K.M, Stevens, B.J, Assamoi, P.J et al. (7 more authors) (2009) Quantum well and dot self-aligned stripe lasers utilizing an InGaP optoelectronic confinement layer. IEEE Journal of Selected Topics in Quantum Electronics, 15 (3). pp. 819-827. ISSN 1077-260X

https://doi.org/10.1109/JSTQE.2008.2011654

Quantum Well and Dot Self-Aligned Stripe Lasers Utilizing an InGaP Optoelectronic Confinement Layer

Kristian M. Groom, *Member, IEEE*, Benjamin J. Stevens, P. Joel Assamoi, John S. Roberts, Maxime Hugues, David T. D. Childs, Ryan R. Alexander, Mark Hopkinson, Amr S. Helmy, *Senior Member, IEEE*, and Richard A. Hogg, *Member, IEEE*

***Abstract*—We demonstrate and study a novel process for fabrication of GaAs-based self-aligned lasers based upon a single overgrowth. A lattice-matched n-doped InGaP layer is utilized for both electrical and optical confinements. Single-lateral-mode emission is demonstrated initially from an $In_{0.17}Ga_{0.83}As$ double quantum well laser emitting ∼980 nm. We then apply the fabrication technique to a quantum dot laser emitting ∼1300 nm. Furthermore, we analyze the breakdown mechanism in our devices and discuss the limitations of index guiding in our structures.**

***Index Terms*—Quantum well (QW) laser, semiconductor device fabrication, semiconductor laser.**

I. Introduction

Lasers based upon the GaAs materials system offer a number of advantages over their InP counterparts, namely the use of larger substrates (>3 in) for reduced fabrication costs and a more favorable band offset enabling higher temperature (or uncooled) operation through improved carrier confinement. Recent developments, such as high-quality dilute nitride quantum wells (QWs) [1] and InAs quantum dots (QDs) at 1.3 μm [2], have brought about the commercialization of GaAs-based optical communication devices. Buried heterostructures and self-aligned stripes are typically utilized in the manufacture of InP telecommunication lasers yielding devices with high reliability, small active widths, high-quality interfaces, reduced nonradiative recombination at exposed surfaces, and control of carrier flow permitting high local current densities for low drive currents, allowing the use of inexpensive drive electronics. Additionally, the flexibility provided by this approach affords narrower and more symmetric far-field emission profiles, thus allowing more efficient fiber coupling.

Epitaxial regrowth in GaAs-based structures is problematic, mainly due to the Al containing layers within the structure, which, when exposed to oxygen, result in poor regrowth interfaces that are deleterious to the laser performance. Previous solutions have included the use of Al-free epitaxial structures [3], steam oxidation for current confinement [4], *in situ* etching and regrowth within a metal–organic vapor phase epitaxy (MOVPE) reactor [5], and antiguided [6], buried ridge [7], or self-aligned structures [8], [9], where Al layers were exposed to oxygen. All these have associated difficulties in process control, reliability, and design flexibility.

In this paper, we demonstrate and study a novel technique for the fabrication of GaAs-based self-aligned lasers utilizing a lattice-matched n-doped InGaP current blocking layer that also provides optical confinement via predominantly index guiding. The key novelty introduced is the simultaneous current and optical confinement due to the InGaP layer. Furthermore, this technology relies upon the careful design of the epitaxial structure to ensure that no $Al_xGa_{1-x}As$ is exposed during the fabrication process, in contrast to [7]–[9]. We combine these ideas in a device structure to avoid issues with oxidizing $Al_xGa_{1-x}As$ layers during device processing. In this paper, we first utilize a 980-nm-QW active region design, as previously introduced in [10]. Such media find widespread application as optical pumps for erbium-doped fiber amplifiers, but is used in this case simply as a robust material for initial investigation. The technology is perhaps better suited for exploitation of long-wavelength QD and dilute nitride technology for application in metro and access data communications. As such, we also investigate a 1.3-μm self-assembled QD self-aligned laser in this paper. Lasers fabricated demonstrate extremely encouraging characteristics, and importantly, the dot emission is shown to be robust to the GaAs/AlGaAs regrowth as no blue-shift is observed, indicating that this technique will be suitable for realizing advanced QD structures, devices, and integrated circuits.

II. Realization of QW Self-Aligned Stripe Laser

A. Device Design and Fabrication

The schematic of our completed device is shown in Fig. 1(a). The basic elements of the device are the combination of p-n-p-n current blocking layers and the refractive index contrast of the GaAs, $Al_{0.42}Ga_{0.58}As$, and InGaP to simultaneously achieve optical and carrier confinement. Fig. 1(b) shows modeling of

Manuscript received October 30, 2008; revised December 4, 2008. Current version published June 5, 2009. This work was supported by the U.K. Engineering and Physical Sciences Research Council (EPSRC) under Grant EP/E001017/1 and by the Royal Academy of Engineering.

K. M. Groom, B. J. Stevens, P. J. Assamoi, J. S. Roberts, M. Hugues, D. T. D. Childs, R. R. Alexander, M. Hopkinson, and R. A. Hogg are with the Department of Electronic and Electrical Engineering, Centre for Nanoscience and Technology, University of Sheffield, Sheffield S3 7HQ, U.K. (e-mail: k.m.groom@sheffield.ac.uk).

A. S. Helmy is with the Department of Electrical and Computer Engineering, University of Toronto, Toronto, ON M5S 3G4, Canada.

Color versions of one or more of the figures in this paper are available online at http://ieeexplore.ieee.org.

Digital Object Identifier 10.1109/JSTQE.2008.2011654

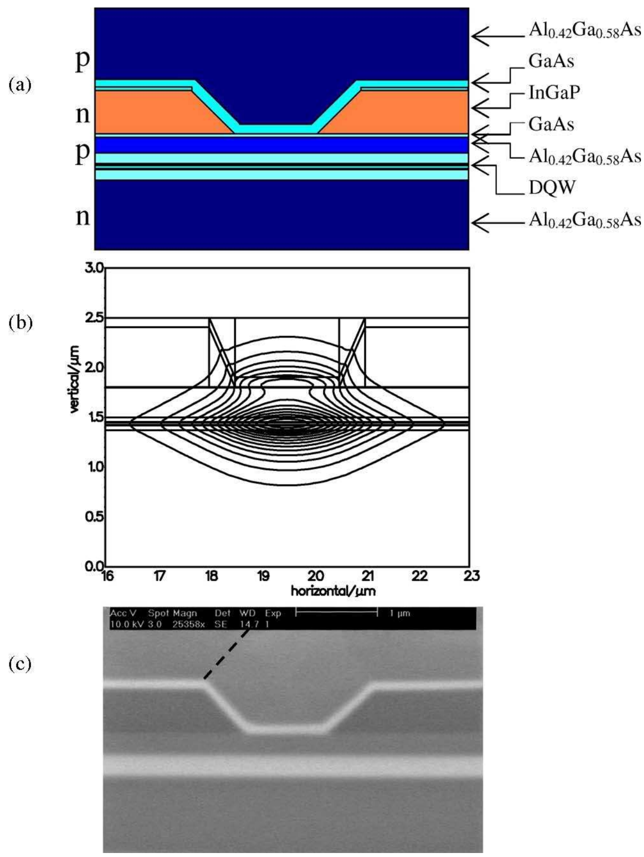

Fig. 1. (a) Schematic diagram to assist in identifying the layers of the self-aligned stripe. (b) Optical mode as modeled in Fimmwave (only index guiding is considered). (c) Cross-sectional SEM of the regrown structure. The dotted line is a guide to the eye for the contrast difference.

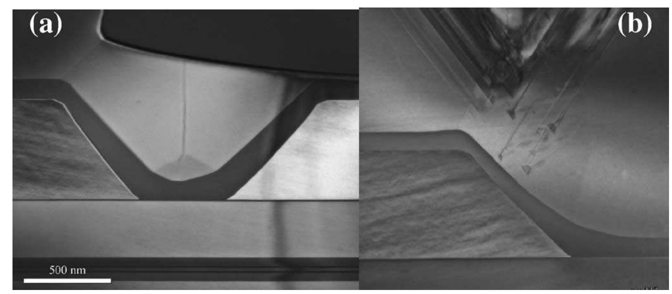

Fig. 2. Cross-sectional dark field 0 0 2 TEM of the overgrown structure at (a) 690 °C and (b) 650 °C. Part of the structure in (a) has been etched back through the top cladding. Supplied by [13].

the fundamental TE mode within the structure using Fimmwave software [11], a development of the film mode matching method for mode solution in dielectric waveguides.

The initial MOVPE epitaxial growth was carried out on a 3°-OFF (1 0 0) n+ GaAs substrate to create a large number of reaction sites due to the greater step density. Following the growth of a GaAs buffer, 1000 nm Si-doped $Al_{0.42}Ga_{0.58}As$ (to a concentration of 5×10^{17} cm^{-3}) lower cladding was grown. The double QW (DQW) active region comprises two $In_{0.17}Ga_{0.83}As$ QWs separated by 20 nm GaAs, grown within a 100 nm GaAs separate confinement heterostructure. Above the active region, 300 nm $Al_{0.42}Ga_{0.58}As$ (Zn-doped 5×10^{17} cm^{-3}) was grown. A 600 nm lattice-matched n-doped InGaP layer (Si-doped 5×10^{17} cm^{-3}) was then sandwiched between two undoped 10 nm GaAs layers, which are sufficiently thin to be doped to a high concentration from residual doping and diffusion. AlGaAs was grown at a thermocouple temperature of 700 °C, InGaP at 710 °C, and the DQW at 680 °C.

The planar wafer was patterned and wet chemically etched (*ex situ*) into a series of narrow stripes parallel to the major flat (1 1 0). Etching proceeded first with $C_6H_8O_7/H_2O_2$ to selectively etch the GaAs, then H_3PO_4/HCl to selectively etch the InGaP, leaving a smooth GaAs surface at the bottom of the stripe. No AlGaAs is exposed. Prior to regrowth, the wafer was cleaned in 1% buffered HF. The low-pressure regrowth process consisted of rapidly ramping up to 690 °C (measured by EpiTT pyrometer) in an arsine mole fraction of 7.5×10^{-3}, before growth of 100 nm GaAs (C-doped 5×10^{17} cm^{-3}), 1000 nm $Al_{0.42}Ga_{0.58}As$ (C-doped from 5×10^{17} to 1×10^{18} cm^{-3}), and a 200 nm GaAs contact layer (C-doped 2×10^{19} cm^{-3}). The material was etched into wide ridges for electrical isolation and AuZnAu contact metallization was deposited and annealed at 360 °C. After thinning the substrate, InGeAu back contacts were deposited and annealed at 340 °C. Key features of this layer structure are the GaAs layers that sandwich the InGaP layer. The lower GaAs layer prevents the exposure of $Al_{0.42}Ga_{0.58}As$ to oxygen during the fabrication process and acts as an etch stop. The upper GaAs layer has two roles: first, preventing an exchange interaction between P and As during the regrowth step, and second, pinning the wet etch employed to define the laser stripe. The thickness and doping concentration of these layers were chosen to minimize current leakage, thus resulting in the current being localized to the area defined by the stripe, while the refractive index profile that these layers provide simultaneously confines the optical field to the active region below the stripe.

A cross-sectional SEM of the completed device is shown in Fig. 1(c). This corresponds to a 500-nm-wide stripe structure. Contrast between the GaAs, $Al_{0.42}Ga_{0.58}As$, and InGaP layers is observed, although the QWs and thin GaAs insertions are not resolved. The image is indicative of the excellent regrowth quality, free from obvious defects. Furthermore, careful inspection of the SEM image reveals a slight contrast difference for the $Al_xGa_{1-x}As$ immediately above the laser stripe, compared to that grown on top of the InGaP layer. This is suggestive of a compositional variation of $Al_xGa_{1-x}As$ grown upon a nonplanar surface [12], Al being depleted above the stripe.

Careful inspection of the dark field 0 0 2 transmission electron micrograph (TEM) image in Fig. 2(a) demonstrates a high-quality interface with no defect or dislocation present. Although part of the structure has been etched away through the upper cladding, there is no evidence of the formation of dislocation "twins." Such twins would be evident in the first ~100 nm of AlGaAs, as they are in the structure overgrown at lower temperature [Fig. 2(b)] and originate almost as soon as the AlGaAs is formed. V-shaped defect clusters are apparent above the edges of the infill region and propagate to the surface of the semiconductor. Dark field 0 0 2 imaging conditions are sensitive to

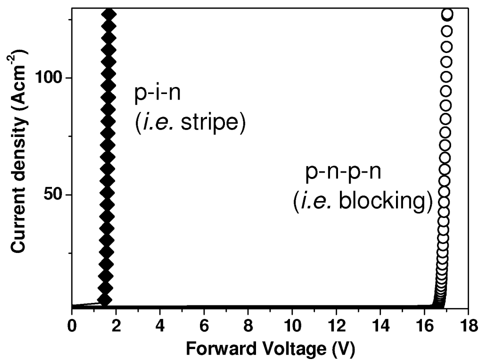

Fig. 3. Current density–voltage characteristics of mesa diodes processed from p-i-n (solid circles) and p-n-p-n (open circles) portions of the wafer.

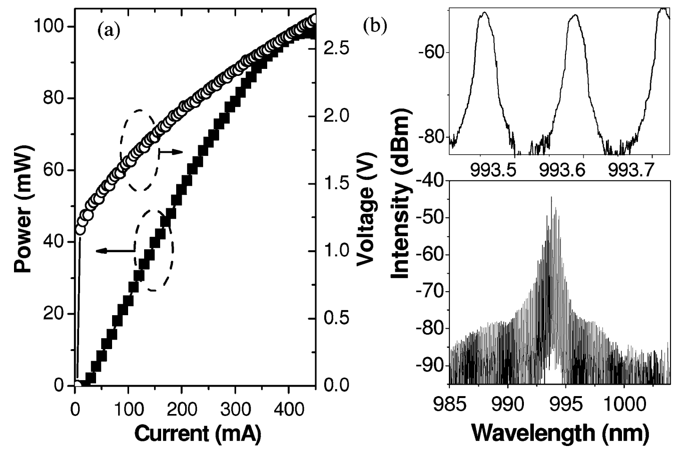

Fig. 4. (a) CW output power and voltage versus current response of a 3-μm-wide stripe laser. (b) Lasing spectrum at (lower) 40 mA CW and (upper) for a portion of the spectrum to demonstrate the absence of competing lateral modes.

composition, revealing important differences in the composition of the overgrown material. In Fig. 2(a), the overgrown GaAs appears to have formed uniformly on all exposed surfaces, and the TEM reveals contrast differences within the $Al_xGa_{1-x}As$ above the laser stripe, indicative of a compositional variation in the $Al_xGa_{1-x}As$ grown above the stripe, and suggests the occurrence of preferential growth in the (1 1 1) directions. This is in addition to the contrast noted in the SEM above which a contrast is identified between the $Al_xGa_{1-x}As$ above the stripe and that outside of the stripe.

B. Results and Discussion

In order to characterize the electrical characteristics of the current blocking layers, 100-μm-diameter circular mesas were processed from portions of the wafer where the InGaP was removed (p-i-n structure) and where the InGaP is left intact (p-n-p-n structure). Fig. 3 plots the current density versus voltage characteristics recorded for these two devices. The p-i-n devices exhibit typical diode characteristics, turning ON at $\sim$1.5 V. The p-n-p-n device exhibits effective current blocking, with a breakdown of the current blocking evidenced by the large increase in current commencing $\sim$17 V. At forward voltages $<$17 V, current flow in the buried heterostructure lasers should therefore be confined to the stripe region.

One-millimeter-long (uncoated) devices were mounted epi-side-up on AlO_2 tiles and tested at room temperature without active cooling. The continuous-wave (CW) output power and voltage versus current responses for a device with a 3-μm-wide aperture in the InGaP is shown in Fig. 4(a), together with a corresponding lasing electroluminescence (EL) spectrum in Fig. 4(b). The threshold current is 20 mA, corresponding to a threshold current density ($J_{\rm th}$) of 666 A·cm^{-2}, calculated without taking into account any current spreading, and hence, provides an upper limit to the value for $J_{\rm th}$. From comparison between different stripe widths (not shown), we estimate the total current spreading as 1 μm. Hence, a more likely $J_{\rm th}$ value of 500 A·cm^{-2} is determined. The maximum CW output power from one facet is 98 mW (limited by thermal rollover), with 0.3 W/A per facet slope efficiency. The higher than expected series resistance $\sim$5 Ω could be a result of the inverted-trapezoidal profile of the blocking layer or carrier leakage.

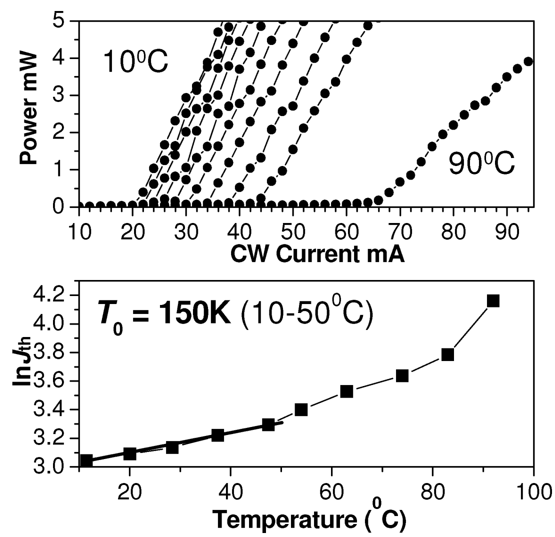

Fig. 5. (a) High-temperature performance of the 980 nm self-aligned laser demonstrated as a series of P versus I curves over the range of temperatures 10 °C–90 °C. (b) $J_{\rm th}$ plotted as a function of temperature. The thick line demonstrates the region 10 °C–50 °C where a T_0 of 150 K is extracted.

The above-threshold EL spectrum exhibits a Fabry–Perot lasing envelope at a central wavelength of 994 nm, with no obvious competition from higher order lateral modes observable in the spectrum (inset).

Devices were tested up to 90 °C (Fig. 5), where CW operation was still achieved with no active cooling. A characteristic temperature T_0 of 150 K is extracted over the range 10 °C–50 °C.

Fig. 6 plots the horizontal and vertical far-field profiles of the device for (a) low current (40 mA) and (b) high current (400 mA), recorded by coupling the light into a standard far-field goniometer with InGaAs detector. The measured low-current divergence angles of 33° vertical and 14.6° horizontal correlate well with those predicted using Fimmwave software [Fig. 6(a)] of 33.3° and 14.4°. The difference in far-field divergence is attributed to uncertainties in the $Al_xGa_{1-x}As$ composition due to regrowth on a patterned surface and the effects of gain guiding in the structure. A wider divergence is observed at higher

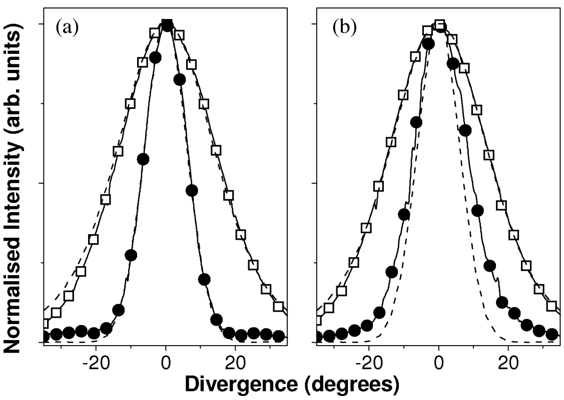

Fig. 6. Horizontal (circles) and vertical (squares) far-field sections for drive currents of (a) 40 mA and (b) 400 mA. Simulated far-field sections are plotted in both figures as dotted lines.

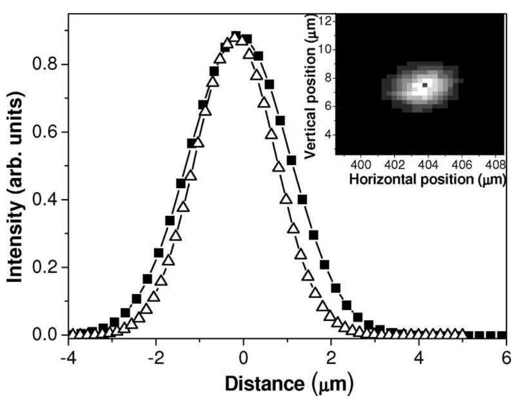

Fig. 7. Experimentally measured horizontal (closed squares) and vertical (open triangles) near-field sections of the far-field profile plotted in the inset.

currents and is attributed to an enhanced contribution of gain guiding. Nearly symmetric far fields (22.2°, 28.7°) were attained for narrower (500 nm wide) stripes.

The device clearly operates on the fundamental lateral mode under all injection conditions, even up to the maximum output power at 400 mA. However, as further proof of the single-lateral-mode nature of the emission, the 2-D near-field profile was scanned using a lensed single-mode optical fiber. The measured lateral and vertical near-field sections are shown in Fig. 7. The inset plots the full 2-D near-field profile.

The near-field optical profile exhibits a single peak. The cone of light is measured to originate from a single $\sim 3\ \mu$m $\times 2\ \mu$m section of the device in the center of the 50-μm-wide device. However, the near-field resolution is of the order of $\sim 2\ \mu$m (limited by the lensed fiber), so while detailed mapping of the near field is not possible, this measurement serves to demonstrate the effective current and optical confinement within the device.

III. Realization of QD Self-Aligned Stripe Laser

A. Device Design

The initial molecular beam epitaxy (MBE) growth was again carried out on a 3°-off (1 0 0) n+ GaAs substrate. Following growth of a GaAs buffer, 1500 nm Si-doped (5×10^{17} cm^{-3})

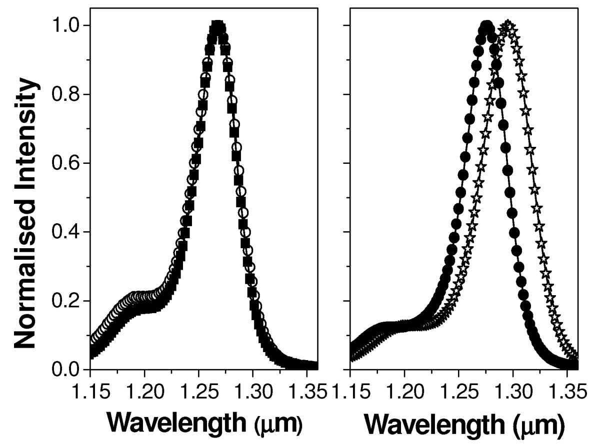

Fig. 8. (a) PL spectrum recorded before and after MOVPE regrowth at room temperature under identical excitation conditions. No blue-shift is observed, with peak identical at 1.27 μm. (b) PL recorded for a similar structure for growth on (1 0 0) and 3° misoriented substrates.

$Al_{0.42}Ga_{0.58}As$ lower cladding was grown (growth temperature $T_g = 620\,^\circ$C). Six InAs QD layers were each capped with a 6 nm $In_{0.15}Ga_{0.83}As$ strain reducing layer ($T_g = 510\,^\circ$C) and separated by 50 nm GaAs spacer ($T_g = 580\,^\circ$C), incorporating a modulation doping layer providing $\sim$12 additional acceptors per dot (situated 25 nm below each dot layer). This was embedded within 100 nm GaAs separate confinement layers. Above the active region, 300 nm $Al_{0.42}Ga_{0.58}As$ (Be-doped 5×10^{17} cm^{-3}, $T_g = 600\,^\circ$C) was grown before a 600 nm lattice-matched Si-doped (5×10^{17} cm^{-3}) InGaP layer ($T_g = 520\,^\circ$C) was sandwiched between two Be-doped 20 nm GaAs layers. These were thicker than for the QW structure only as part of an experiment investigating native oxide removal.

Again, the planar wafer was patterned and selectively wet-etched (*ex situ*) through the InGaP into a range of narrow stripes, leaving a smooth GaAs surface at the bottom of each stripe, and the regrowth process consisted of ramping up to the growth temperature in an arsine environment, before growth of 100 nm GaAs, 1500 nm $Al_{0.42}Ga_{0.58}As$, and 200 nm GaAs contact layer (C-doped 5×10^{17} to 1×10^{18} cm^{-3} to 2×10^{19} cm^{-3}, respectively). Broad-area (20–50 μm) ridges were again etched for the purpose of electrical isolation and contacts were applied as before.

B. Photoluminescence (PL) Characterization

Room-temperature PL spectra were recorded from the material under identical excitation conditions before and after the MOVPE regrowth, and are plotted in Fig. 8. No blue-shift of the QD emission, which peaks at 1.27 μm, is observed. QD emission wavelength has previously been shown to shorten as a result of annealing at temperatures similar to those used in the MOVPE regrowth of our structures, e.g., [14]. In such cases, Ga vacancies are either present or they are created during the anneal process, and are often enhanced through use of sputtered or plasma-enhanced CVD (PECVD) SiO_2 layers [15]. The presence of Ga vacancies close to the dots allows the outdiffusion of In, resulting in a blue-shift. In our structures, growth is

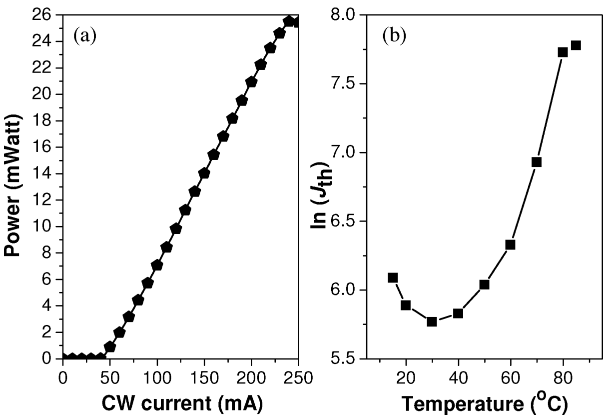

Fig. 9. (a) Output power as a function of CW current for 5-μm-wide stripe, 1-mm-long laser. (b) Temperature dependence of $J_{\rm th}$.

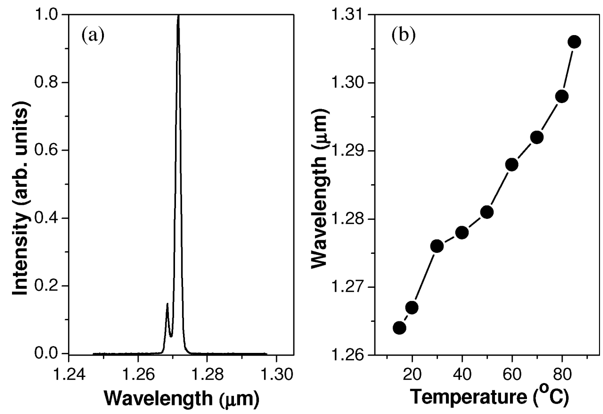

Fig. 10. (a) Low-resolution room-temperature lasing EL spectrum (lasing centered at 1.27 μm). (b) Wavelength is plotted as a function of temperature.

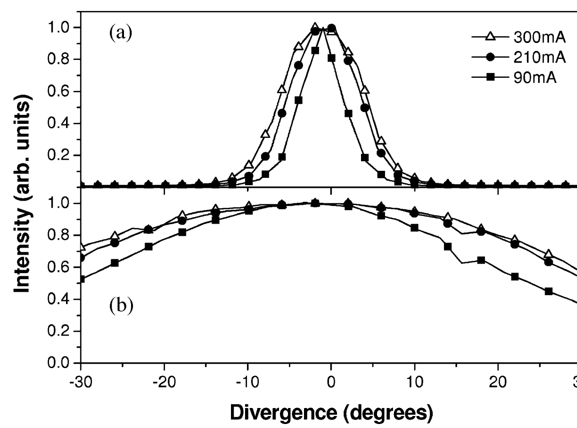

Fig. 11. Far-field profiles (pulsed injection, room temperature) of the device at 90, 210, and 300 mA in the (a) horizontal and (b) vertical directions. All demonstrate emission only from the fundamental mode.

initiated rapidly after thermally cleaning the surface in an attempt to control point defect diffusion.

The active region design used in this study exhibits emission at 1.3 μm when grown on (1 0 0) substrates. However, the requirement of 3° misoriented substrates for high-quality MOVPE regrowth has the result of shortening the emission wavelength compared to the ON-axis case, as demonstrated in Fig. 8(b), recorded for a similar sample where the PL peak wavelength reduced from 1.3 to 1.28 μm. This could be a result of an increased number of steps in the substrate that would manifest itself in an increased dot density and shorter wavelength, and/or the potential to change the shape of the dots. The impact on laser gain and efficiency will be studied elsewhere.

C. Laser Performance

One-millimeter-long (uncoated) devices were tested as a function of temperature. Room-temperature CW output power–current response for a device with a 5-μm-wide stripe in the InGaP is shown in Fig. 9(a). The threshold current is 40 mA. A threshold current density $J_{\rm th}$ of 300 A·cm^{-2} is calculated without taking into account any current spreading, hence providing an upper limit to its value. The maximum CW output power from one facet is 25.5 mW (limited by thermal rollover), with 0.14 W/A slope efficiency.

Devices were tested under pulsed injection up to 90 °C [Fig. 9(a)], where a negative characteristic temperature T_0 was observed around room temperature. Such negative T_0 is typical of QD lasers. The excellent temperature performance of the present lasers highlights the high-quality material grown, despite being grown OFF-axis and suggests an improvement in temperature performance, most probably as a result of surrounding the active waveguide with semiconductor.

The above-threshold room-temperature EL spectrum (recorded at $2J_{\rm th}$) is shown in Fig. 10(a) together with a plot of the lasing wavelength as a function of temperature between 10 °C and 90 °C. The room-temperature EL exhibits a central wavelength of 1270 nm and the device continues to operate via the ground state transition over the range of temperatures studied. This is characterized by the continuous increase in wavelength as a function of temperature. For devices shorter than 1 mm, lasing proceeded via an excited state transition. This was also the case for ridge waveguide devices processed from identical material (not shown here), and suggests that the internal losses are very similar.

Fig. 11 plots the horizontal (a) and vertical (b) far-field profiles of the device for a range of drive currents at room temperature using a standard far-field goniometer with InGaAs detector. The measured low-current divergence of 55° (vertical) and 6° (horizontal) increase to 72° and 11° at high current as a result of enhanced gain guiding. This QD self-aligned laser was not designed for optimum far-field profile, and exhibits strong asymmetry typical of narrow lasers with relatively high Al composition cladding.

The device operates on the fundamental lateral mode under all injection conditions studied, even up to the maximum output power at 300 mA. Such single-lateral-mode behavior is further evidenced through scanning a single-mode optical fiber to obtain the near-field profile. The near-field profile plotted in Fig. 12 exhibits a single peak, with the cone of light originating from a single ~7 μm ×7 μm section of the device, in the center of the 50-μm-wide ridge. However, this is of the order of the resolution of the scanning fiber (no lens), so while detailed mapping of the

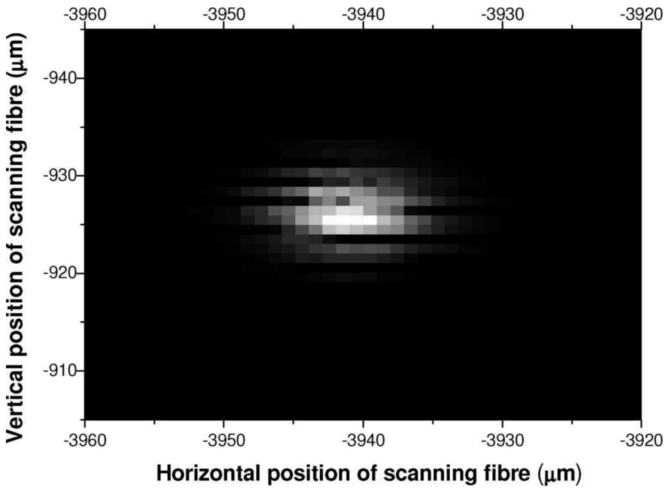

Fig. 12. Experimentally measured room temperature near-field profile at 120 mA (CW) with resolution limited ~7 μm full width at half maximum (FWHM) in both directions.

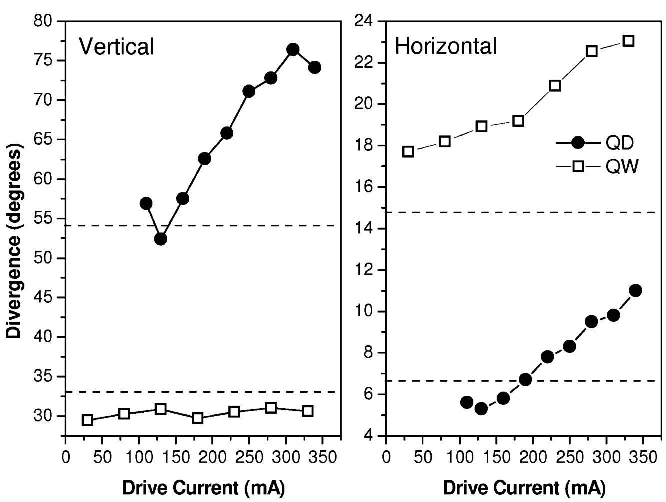

Fig. 13. Experimental horizontal and vertical far-field divergences plotted as a function of drive current for 2 μm QD and QW self-aligned lasers. Dashed lines represent simulated divergences.

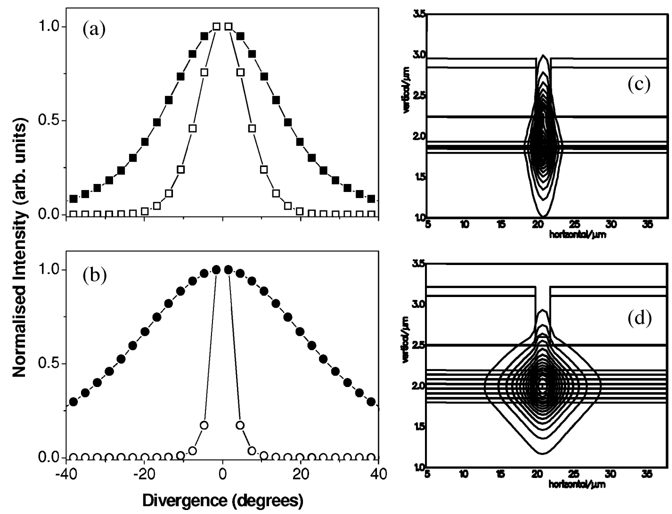

Fig. 14. Modeled horizontal and vertical far-field divergences plotted as a function of drive current for 2-μm-wide stripe (a) QW and (b) QD self-aligned stripe lasers. Corresponding modeled near-field profiles are plotted in (c) and (d) for QW and QD, respectively, superimposed on the simulated layer structure. The sloped InGaP profile is approximated as vertical for computational efficiency—there is negligible difference compared with inclusion of slopes.

near field was not possible, the measurement demonstrates the effective current and optical confinement within the device, i.e., the device operates as a single-spatial-mode self-aligned laser rather than as a broad-ridge laser.

The QD self-aligned laser exhibits a notably different far-field profile when compared to that observed in their QW counterparts studied in [10] in terms of the asymmetry and its dependence upon drive current. This is demonstrated in Fig. 13 for 2-μm-wide stripes, which both operate on the fundamental lateral mode over the whole current range. For the QW laser, the divergences are $\sim 18^\circ$ horizontal and 30° vertical just above threshold. There is then a gradual increase in the horizontal divergence as a function of current above threshold. For the QD laser, the horizontal and vertical divergences are $\sim 6^\circ$ and 55°, respectively, and a more prominent increase in far-field divergence is observed with increasing drive current.

These differences can be explained through waveguide simulation. In addition to their different emission wavelengths, the QD structures have a wider active core (~450 nm) resulting in narrower vertical divergence compared to the QW structures (~135 nm). These have an effect on the effective refractive index profiles of the two structures and hence the optical confinement. This is demonstrated in Fig. 14, which shows horizontal and vertical far-field profiles simulated for QW (a) and QD (b) self-aligned stripe lasers of 2 μm stripe width. The QD laser is predicted to yield divergences of 6.7° and 54° in the horizontal and vertical directions, respectively, while the QW laser is predicted to yield divergences of 14.7° and 33°. These are superimposed as dashed lines in Fig. 13.

The simulated optical near fields are shown in Fig. 14(c) and (d) for QW and QD self-aligned stripe lasers, respectively. For the QD laser, the optical mode is positioned lower down in the structure than for the QW, resulting in reduced overlap of the mode to the index differential created by the stripe, and hence, less confined in the lateral direction, thus resulting in narrower lateral divergence. As a consequence, the QD laser should experience a greater relative contribution of gain guiding and is hence more dependent upon drive current. This result implies that there are important limitations to the usefulness of this approach for wide active core structures such as those utilizing QDs.

IV. Breakdown of Current Blocking

Fig. 15 demonstrates the mechanism behind the electrical breakdown of current blocking in self-aligned lasers in forward bias, in this case for a QW laser of length 1 mm and 1 μm stripe width. The P–I curve exhibits an abrupt decrease in power with increasing drive current. Further increase in current results in a modest increase in power before the device exhibits thermal

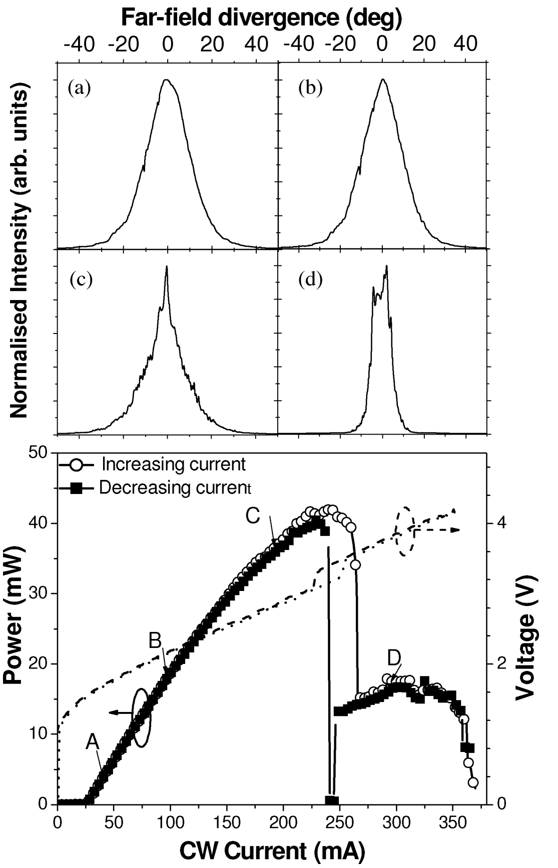

Fig. 15. Breakdown hysteresis effect demonstrated for a 1-mm-long, 1-μm-wide stripe. Step changes in I–V and P–I curves are accompanied by a commensurate change in the horizontal divergence (top).

rollover. With decreasing current, the power reduces to 0.5 mW before recovering to prebreakdown levels exhibiting a 25 mA hysteresis. The reason for the marked decrease in power before the power recovers is unknown.

To illustrate the reason for the form of the P–I horizontal far fields were measured and are shown for various points on the curve. The far fields for points A and B on the curve have a shape that is consistent with lasing occurring only from the section defined by the stripe rather than the 8 μm ridge in which the stripe is positioned. As the current is increased further, the power continues to increase. However, by point C, the far field is beginning to narrow, suggesting degradation in the current confinement manifesting itself in a narrower far field. By point D, there has been a total breakdown of the current confinement and the far field is consistent with the device lasing from the 8 μm ridge that provides electrical isolation between the ridges.

The current blocking in self-aligned stripe lasers is expected to eventually breakdown, permitting current flow across the whole ridge that is used to isolate devices and manifesting itself in a narrowing of the horizontal far-field divergence. At the breakdown point, the voltage across the device increases as the breakdown occurs and reduces as the current blocking recovers. Fig. 3 suggests that breakdown should not occur until a voltage of $\sim$18 V has been applied; however, for the laser devices in Fig. 15, breakdown occurs $\sim$3.5 V. We attribute the lower breakdown voltage of the laser device compared to mesa devices to the 54° etch profile of the InGaP stripe causing local high-electric-field regions allowing breakdown to occur at lower voltages. Such a change in far field could be exploited as a possible modulation scheme and also offers the possibility of a variable divergence laser.

V. Conclusion

In summary, we have demonstrated a novel GaAs-based self-aligned laser in both 980 nm QW and 1300 nm QD schemes. Careful design in order to avoid the exposure of Al containing alloys is combined with an InGaP current blocking and optical confinement layer to result in single-lateral-mode behavior. This single-overgrowth design offers a simple manufacturable method for single-lateral-mode lasers on GaAs substrates. Furthermore, we have described the limitations of both index guiding and current blocking in our design.

References

[1] N. Tansu, J. Y. Yeh, and L. J. Mawst, "High-performance 1200 nm InGaAs and 1300 nm InGaAsN quantum well lasers by metalorganic chemical vapour deposition," *IEEE J. Sel. Topics Quantum Electron.*, vol. 9, no. 5, pp. 1220–1227, Sep./Oct. 2003.

[2] R. R. Alexander, D. T. D. Childs, H. Agarwal, K. M. Groom, H. Y. Liu, M. Hopkinson, R. A. Hogg, M. Ishida, T. Yamamoto, M. Sugawara, Y. Arakawa, T. J. Badcock, R. J. Royce, and D. J. Mowbray, "Systematic study of the effects of modulation p-doping on 1.3 μm quantum dot lasers," *IEEE J. Quantum Electron.*, vol. 43, no. 12, pp. 1129–1139, Dec. 2007.

[3] N. T. Yeh, W. S. Liu, S. H. Chen, P. C. Chiu, and J. I. Chyi, "InAs/GaAs quantum dot lasers with InGaP cladding layer grown by solid source molecular beam epitaxy," *Appl. Phys. Let.*, vol. 80, no. 4, pp. 535–537, 2002.

[4] F. A. Kish, S. J. Caracci, N. Holonyak, Jr., J. M. Dallesasse, K. C. Hsieh, and M. J. Ries, "Planar native-oxide index-guided $Al_x Ga_{1-x} As$ quantum well heterostructure lasers," *Appl. Phys. Let.*, vol. 59, no. 14, pp. 1755–1757, 1991.

[5] M. Nido, I. Komazaki, K. Kobayashi, K. Endo, M. Ueno, T. Kamejima, and T. Suzuki, "AlGaAs/GaAs self-aligned LD's fabricated by the process containing vapour phase etching and subsequent MOVPE regrowth," *IEEE J. Quantum Electron.*, vol. QE-23, no. 6, pp. 720–724, Jan. 1987.

[6] L. J. Mawst, H. Yang, M. Nesnidal, A. Al-Muhanna, D. Botez, T. A. Vang, F. D. Alvarez, and R. Johnson, "High-power, single mode, Al-free InGaAs(P)/InGaP/GaAs distributed feedback diode lasers," *J. Cryst. Growth*, vol. 195, pp. 609–616, 1998.

[7] S. Ishikawa, K. Kukagai, H. Chida, T. Miyazaki, H. Fujii, and K. Endo, "0.98–1.02 μm strained InGaAs/AlGaAs double quantum well high-power lasers with GaInP buried waveguides," *IEEE J. Quantum Electron.*, vol. 29, no. 6, pp. 1936–1942, Jun. 1993.

[8] T. Onishi, O. Imafuji, T. Fukuhisa, A. Mochida, Y. Kobayashi, M. Yuri, K. Itoh, and H. Shimizu, "Monolithically integrated 780 nm-band high-power and 650 nm-band laser diodes with real refractive index guided self-aligned structure," *IEEE Photon. Technol. Lett.*, vol. 13, no. 6, pp. 550–552, Jun. 2001.

[9] J. J. Coleman and P. D. Dapkus, "Single-longitudinal-mode metalorganic chemical-vapour-deposition self-aligned GaAlAs-GaAs double-heterostructure lasers," *Appl. Phys. Lett.*, vol. 37, no. 3, pp. 262–263, 1980.

[10] K. M. Groom, B. J. Stevens, R. R. Alexander, D. T. D. Childs, A. B. Krysa, J. S. Roberts, A. S. Helmy, and R. A. Hogg, "GaAs-based self-aligned laser incorporating InGaP opto-electronic confinement layer," *Electron. Lett.*, vol. 44, no. 15, pp. 905–906, 2008.

[11] Fimmwave software by Photon Design. (2008). [Online]. Available: http://www.photond.com

[12] M. Walther, E. Kapon, J. Christen, D. M. Hwang, and R. Bhat, "Carrier capture and quantum confinement in GaAs/AlGaAs quantum wire lasers grown on V-grooved substrates," *Appl. Phys. Lett.*, vol. 60, no. 5, pp. 521–523, 1992.

[13] R. Beanland. (2008). TEM analysis, Integrity Scientific Ltd., U.K. [Online]. Available: www.integrityscientific.com

[14] T. Yang, J. Tatebayashi, K. Aoki, M. Nishioka, and Y. Arakawa, "Effects of rapid thermal annealing on the emission properties of highly uniform self-assembled InAs/GaAs quantum dots emitting at 1.3 μm," *Appl. Phys. Lett.*, vol. 90, pp. 111912-1–111912-3, 2007.

[15] N. Y. Gordeev, W. K. Tan, A. C. Bryce, I. I. Novikov, N. V. Kryzhanovskaya, S. M. Kuznetsov, A. G. Gladyshev, M. V. Maximov, S. S. Mikhrin, and J. H. Marsh, "Broad-area InAs/GaAs quantum dot lasers incorporating intermixed passive waveguide," *Electron. Lett.*, vol. 43, no. 1, pp. 29–30, 2007.

Kristian M. Groom (M'05) received the M.Phys. and Ph.D. degrees from the Department of Physics and Astronomy, University of Sheffield, Sheffield, U.K., in 1999 and 2003, respectively.

He is currently with the Department of Electronic and Electrical Engineering, University of Sheffield. He has authored or coauthored more than 40 refereed papers. His current research interests include long-wavelength GaAs-based lasers and superluminescent diodes such as those based on quantum dots.

Dr. Groom was awarded a Royal Academy of Engineering/U.K. Engineering and Physical Sciences Research Council (EPSRC) Fellowship in 2005 for research into advanced semiconductor laser engineering.

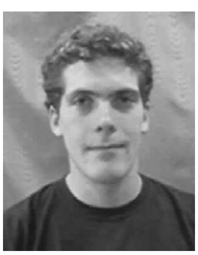

Benjamin J. Stevens received the M.Eng. degree in electronic engineering with a modern foreign language (German) in 2005 from the University of Sheffield, Sheffield, U.K., where he is currently working toward the Ph.D. degree in quantum dot laser and superluminescent diodes.

P. Joel Assamoi was born in Abidjan, Ivory Coast, in 1988. He is currently working toward the Master's degree in electronics and communication engineering at the University of Sheffield, Sheffield, U.K.

He investigated quantum dot self-aligned lasers during a summer research placement.

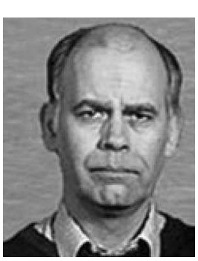

John S. Roberts received the Applied Chemistry degree from the University of Salford, Salford, U.K., in 1971 and the Ph.D. degree in radiation chemistry from the University of Newcastle upon Tyne, Tyne and Wear, U.K., in 1975.

From 1975 to 1980, he was with Philips Research Laboratories, Redhill, U.K., where he was engaged in developing the molecular beam epitaxy (MBE) growth of GaInP for laser applications. Since 1980, he has been with the U.K. Engineering and Physical Sciences Research Council (EPSRC) National Centre for III–V Technologies, University of Sheffield, Sheffield, U.K., where he is currently responsible for the metal–organic vapor phase epitaxy (MOVPE) growth of arsenide and phosphide materials.

Maxime Hugues received the M.Sc. degree in material and device physics from Joseph Fourier University, Grenoble, France, in 2004 and the Ph.D. degree in applied physics from Nice–Sophia Antipolis University, Nice, France, in 2007.

He was with Nice–Sophia Antipolis University, where he mainly worked on dilute nitride and InAs quantum dots for long-wavelength GaAs-based lasers. He is currently with the Department of Electronic and Electrical Engineering, University of Sheffield, Sheffield, U.K., where he is also engaged in the III–V nanostructures growth by molecular beam epitaxy (MBE) at the Engineering and Physical Sciences Research Council (EPSRC) National Centre for III–V Technologies.

David T. D. Childs received the B.Sc. degree in physics, the M.Sc. degree in semiconductor science and technology, and the Ph.D. degree on properties and applications of 1.3-μm InAs/GaAs quantum dots from Imperial College, London, U.K., in 1996, 1997, and 2002, respectively.

Until 2006, he was with the R&D Department, Bookham (formerly Marconi Optical Components), where he was at the Caswell Semiconductor Research and Fabrication Facility, and was responsible for many aspects of the design and characterization of improved active and tuning regions for DFB and multisection tunable DBR laser devices. He was also involved in the European Union (EU) research programs: self-assembled nanostructured materials for electronic and optoelectronic applications (NANOMAT), self-assembled semiconductor nanostructures for new devices in photonics and electronics (SANDIE), and zero order dimension based industrial components applied to telecommunications (ZODIAC). He then joined the Department of Electronic and Electrical Engineering, University of Sheffield, Sheffield, U.K., as a Research Associate (RA), and was engaged in improving quantum dot (QD) laser performance. He is currently involved in the EU program Compact Ultrafast Laser Sources Based on Novel Quantum Dot Structures (FASTDOT) with the aim of implementing a new range of ultrafast quantum-dot lasers for critical biophotonics and medical applications.

Ryan R. Alexander received the B.Sc. degree in physics and electronics in 1998 from the Department of Physics and Astronomy, University of Sheffield, Sheffield, U.K., where he is currently working toward the Ph.D. degree on InAs–GaAs based 1.3 μm quantum-dot lasers at the Department of Electronic and Electrical Engineering.

In 2006, he held a Japan Society for the Promotion of Science (JSPS) Summer Fellowship at the University of Tokyo, Tokyo, Japan.

Mark Hopkinson received the B.Sc. degree in physics from the University of Birmingham, Birmingham, U.K., in 1986 and the Ph.D. degree in physics from the University of Sheffield, Sheffield, U.K., in 1990.

He is a leader of a research group involved in the development of III–V epitaxial nanostructures by molecular beam epitaxy (MBE), with emphasis on novel optoelectronic devices. He was a Postdoctoral Researcher at Warwick University and also at the University of Sheffield, Sheffield, U.K. He then joined Marconi PLC as a Senior Process Engineer. In 2002, he returned to the University of Sheffield and was the Chair in Electronic Engineering in 2007. He has 17-year experience, with over 450 research publications and a wide range of research interactions. His current research interests include III–V quantum dot materials and novel quantum well systems, including antimonide-based structures and dilute nitride materials.

Amr S. Helmy (M'99–SM'06) received the B.Sc. degree in electronics and telecommunications engineering from Cairo University, Cairo, Egypt, in 1993, and the M.Sc. and Ph.D. degrees in photonic fabrication technologies from the University of Glasgow, Glasgow, U.K., in 1994 and 1999, respectively.

He was with the R&D Division, Agilent Technologies Photonic Devices, U.K., where he was engaged in developing distributed feedback lasers, monolithically integrated lasers, modulators, and amplifiers in InP-based semiconductors. He also developed high-powered submarine-class 980-nm InGaAs pump lasers. He is currently an Assistant Professor in the Department of Electrical and Computer Engineering, University of Toronto, Toronto, ON, Canada. His current research interests include photonic device physics and characterization techniques, with emphasis on nonlinear optics in III–V semiconductors, applied optical spectroscopy in III–V optoelectronic devices and materials, and III–V fabrication and monolithic integration techniques.

Dr. Helmy is a member of the Optical Society of America.

Richard A. Hogg (M'04) received the Ph.D. degree from the University of Sheffield, Sheffield, U.K., in 1995.

He was a Postdoctoral Researcher at Nippon Telegraph and Telephone (NTT) Basic Research Laboratories, Atsugi, Japan, for two years. He was then awarded a European Union (EU)–Japan Fellowship as a Visiting Researcher at the University of Tokyo. He was then with Toshiba Research Europe's Cambridge Laboratory for three years. In 2000, he moved to Agilent Technologies Fibre-Optic Component Operation. In 2003, he was appointed as a Senior Lecturer in Semiconductor Devices in the Department of Electronic and Electrical Engineering, University of Sheffield. His current research interests include quantum dot selective area epitaxy, quantum dot devices such as lasers and superluminescent diodes, and quantum cascade DFBs. He has authored or coauthored more than 50 papers and holds 12 patents.